



## OPEN

# Broadband light absorption enhancement in dye-sensitized solar cells with Au-Ag alloy popcorn nanoparticles

## SUBJECT AREAS:

APPLIED PHYSICS

PHYSICS

SOLAR ENERGY AND  
PHOTOVOLTAIC  
TECHNOLOGY

NANOPARTICLES

Qi Xu, Fang Liu, Yuxiang Liu, Kaiyu Cui, Xue Feng, Wei Zhang &amp; Yidong Huang

Department of Electronic Engineering, Tsinghua National Laboratory for Information Science and Technology, Tsinghua University, Beijing 100084, China.

Received

5 February 2013

Accepted

10 June 2013

Published

2 July 2013

Correspondence and requests for materials should be addressed to F.L. (liu\_fang@mail.tsinghua.edu.cn)

In this paper, we present an investigation on the use of Au-Ag alloy popcorn-shaped nanoparticles (NPs) to realise the broadband optical absorption enhancement of dye-sensitized solar cells (DSCs). Both simulation and experimental results indicate that compared with regular plasmonic NPs, such as nano-spheres, irregular popcorn-shaped alloy NPs exhibit absorption enhancement over a broad wavelength range due to the excitation of localized surface plasmons (LSPs) at different wavelengths. The power conversion efficiency (PCE) of DSCs is enhanced by 16% from 5.26% to 6.09% by incorporating 2.38 wt% Au-Ag alloy popcorn NPs. Moreover, by adding a scattering layer on the exterior of the counter electrode, the popcorn NPs demonstrate an even stronger ability to increase the PCE by 32% from 5.94% to 7.85%, which results from the more efficient excitation of the LSP mode on the popcorn NPs.

In recent years, dye-sensitized solar cells (DSCs) have attracted increasing interest due to their relatively high efficiency and low cost of component materials<sup>1–4</sup>. One of the most effective ways to further improve the device efficiency is to increase the light absorption of the photoanodes over a broad range of wavelengths. It is estimated that to obtain a power conversion efficiency (PCE) over 15%, DSCs are required to absorb 80% of sunlight from 350 nm to 900 nm<sup>5</sup>. Plasmonic nanoparticles (NPs) have been employed as a promising approach to boost the light absorption of DSCs due to the localized surface plasmon (LSP) effect<sup>6–12</sup>. Plasmonic NPs incorporated into the photoanode of DSCs can effectively trap incident light to significantly enhance the light absorption of dye molecules and consequently increase the overall efficiency of devices<sup>13–19</sup>. Plasmonic core-shell nano-spheres, such as Au@SiO<sub>2</sub>, Ag@TiO<sub>2</sub>, and Au@PVP, have been employed in DSCs and have exhibited a high absorption enhancement<sup>20–22</sup>. Furthermore, panchromatic DSCs with a TiO<sub>2</sub>-Au-TiO<sub>2</sub> nanostructure have been reported, and their LSP feature could be altered by adjusting the Au-shell thickness<sup>23</sup>. However, metal nano-spheres of a particular size exhibit a relatively narrowband LSP enhancement feature due to the spherical structure of the particles, which cannot support the LSP mode over a wide range of wavelengths. To broaden the LSP enhancement spectrum, Au nano-rods were synthesised and introduced into DSCs, which exhibit two LSP resonance peaks due to the different LSP frequencies along the long and short axes of the nano-rods<sup>24</sup>. Because the excitation of the LSP mode is related to the shape, scale, and material of the corresponding nano-structures<sup>25</sup>, it is anticipated that irregular NPs with many fine structures are possible to support the LSP modes over a wide wavelength range and to enhance broadband light absorption in solar cells.

In this study, plasmonic Au-Ag alloy “popcorn-shaped” core-shell nanoparticles (hereafter referred to as “popcorn NPs”) were proposed and realised by a convenient two-step synthesis method. These plasmonic popcorn NPs exhibit broadband LSP resonance from 350–800 nm. It was demonstrated that by introducing the popcorn NPs with an optimised concentration of 2.38 wt%, the PCE of DSCs was improved by 16%, from 5.26% to 6.09%. Moreover, by adding a scattering layer on the exterior of the counter electrode, the plasmonic enhancement effect is much more significant and the PCE of DSCs can be improved by 32%, from 5.94% to 7.85%. The measured incident photon-to-electron conversion efficiency (IPCE) indicates that an improvement in efficiency is observed over the entire solar spectrum, especially in the range of 500–800 nm.

## Results

The schematic structure of plasmonic-enhanced DSCs with Au-Ag alloy popcorn NPs embedded in the mesoporous TiO<sub>2</sub> layer is shown in Fig. 1. The popcorn NP has several fine structures of different shape, size, and materials (different proportion of Ag and Au) upon which various LSP modes of different wavelengths,

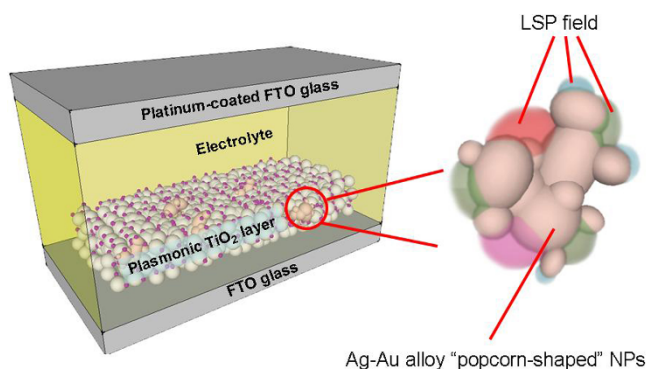


**Figure 1** | Schematic structure of plasmonic enhanced dye-sensitized solar cells (DSCs) with Au-Ag alloy popcorn NPs. Popcorn NPs have several fine structures of different shape and size upon which various LSP modes of different wavelengths, polarisations and field patterns could be excited simultaneously.

polarisations, and field patterns could be excited simultaneously. This effect is expected to increase the optical absorption of dye molecules over a broad range of wavelengths and to enhance the PCE of DSCs.

To investigate the light trapping effect of the popcorn NPs in the LSP mode, a two-dimensional (2D) model rather than a 3D model was established based on the finite element method (FEM)<sup>26</sup> for simplicity (see Methods). The incident light is set to illuminate from one and two directions, respectively, which could help us understand the real situation when popcorn NPs in plasmonic DSCs are illuminated by light from different directions. Figure 2 shows the intensity of the electrical field  $|E|^2$  of an irregular “popcorn-shaped” Au NPs in the  $\text{TiO}_2$  layer with an incident plane wave. The colour bar shows the intensity normalised by the maximum. Figures 2(a)–(c) show the LSP field distribution of the popcorn NP with incident light with wavelengths of 490 nm, 650 nm and 790 nm, respectively. It is illustrated that different LSP modes are excited at different parts of the popcorn NP at different wavelengths. In actual DSCs, a scattering layer or reflective film is usually applied to enhance light absorption by reflecting and scattering the incident light back into the active layer<sup>27,28</sup>. Therefore, Fig. 2(d)–(f) assumes that the popcorn NP is irradiated by light from both the top and bottom with the same intensity and polarisation, which can simulate the case in which there is back-reflected light. It is illustrated that more LSP modes are excited simultaneously on the popcorn NPs due to various fine structures. This result implies that, when a popcorn NP is irradiated by incident light in different directions, the LSP modes will be excited more efficiently and the particle will exhibit better light trapping, which can be confirmed by the experimental results shown later. It should be noted that we employed solely Au instead of Au/Ag alloy for simplicity, while popcorn NPs, in actuality, are much more complex due to the use of different proportion of Au-Ag alloy, which enhances the excitation of LSP modes over a wide range of wavelengths.

By utilising a modified two-step co-reduction method (the details can be found in the Methods), we obtained irregular, asymmetrical Ag-Au alloy popcorn NPs instead of regular nano-spheres or nano-rods (See Fig. S1, Supporting information). Such particles are obtained because the redox potential of Au is much higher than that of Ag<sup>29</sup>. In the first step, Au and Ag ions are reduced at different rates, and the diffusion of these two metals is incomplete, which results in the formation of irregular Ag-Au alloy NPs. Additionally, the boiling solution and additional reductant help reduce the rest of the Ag ions to Ag atoms (a few Au ions are also reduced), which accumulate on the irregular alloy NPs’ surface. The silver shell on the surface of NPs can be easily oxidised to silver oxide in air, which leads to the formation

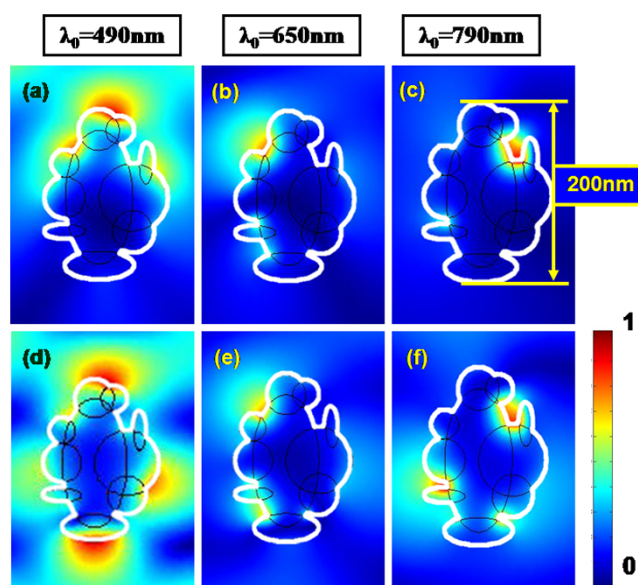


**Figure 2** | Theoretical investigation of the localized surface plasmon (LSP) effect of the popcorn NPs. For simplicity, we use a 2D model instead of a 3D model and assume the popcorn NP model to be a large ellipsoidal structure (approximately 180 nm) with several small ellipsoidal structures (approximately 20–50 nm) on it. (a) to (c): The LSP field distribution of the popcorn NP illuminated by incident light in one direction at wavelengths of (a) 490 nm, (b) 650 nm and (c) 790 nm, respectively. (d) to (f): The LSP field distribution of the popcorn NP illuminated by incident light in two opposite directions at wavelengths of (d) 490 nm, (e) 650 nm and (f) 790 nm, respectively.

of a thin silver oxide shell to protect the popcorn NPs from the iodide electrolyte. Furthermore, utilising Au and Ag as the plasmonic materials simultaneously has two benefits. First, popcorn NPs with different proportions of Ag and Au in different parts can be obtained, which results in the excitation of various LSP modes over a wide range of wavelengths. Secondly, irregular plasmonic nanostructures can be readily obtained due to the different redox potentials of Au and Ag.

Figure 3(a) shows a scanning electron microscopy (SEM) image of popcorn NPs. The average size of the NPs is approximately  $200 \pm 50$  nm, with many irregular fine structures on the nanoscale and a  $\sim 2$  nm  $\text{Ag}_2\text{O}$  shell. The energy dispersive spectroscopy (EDS) of the popcorn NPs shown in Fig. 3 (b) indicate the characteristic peaks of Ag, Au, and O, which represent the components of the NPs (see Fig. S2, Supporting information). The other peaks (from left to right: C, Cu, Al and Cu) in the EDS spectra are due to the carrier and clamp used in SEM measurements. To be noticed, popcorn NPs with different proportions of Ag and Au in different parts were observed, as shown in 1# and 2# in Fig. 3 (b). Optical absorption spectroscopy measurements were performed using a UV-visible spectrophotometer (HITACHI U-3010). Figure 3(d) shows the optical absorption spectra of popcorn NPs dispersed in ethanol before/after being mixed with a iodide/triiodide redox couple-based electrolyte, where the peak at approximately 410 nm (red line) should be from elements composing the electrolyte (see Methods). Because the popcorn NPs possess various fine structures on the nanoscale, the black line in Fig. 3(d) indicates the broadband light absorption at 400 nm, and correspondingly, the solution of NPs (sample 1) in Fig. 3(c) exhibits a dark yellow colour. When mixed with the iodide electrolyte, the alloy NPs also appear to be opaque (sample 2), indicating that the  $\text{Ag}_2\text{O}$  shell could protect the NPs from the electrolyte of DSCs, which is also indicated by the red curve in Fig. 3(d) showing the broad optical absorption spectrum of popcorn NPs. To investigate the LSPs effect

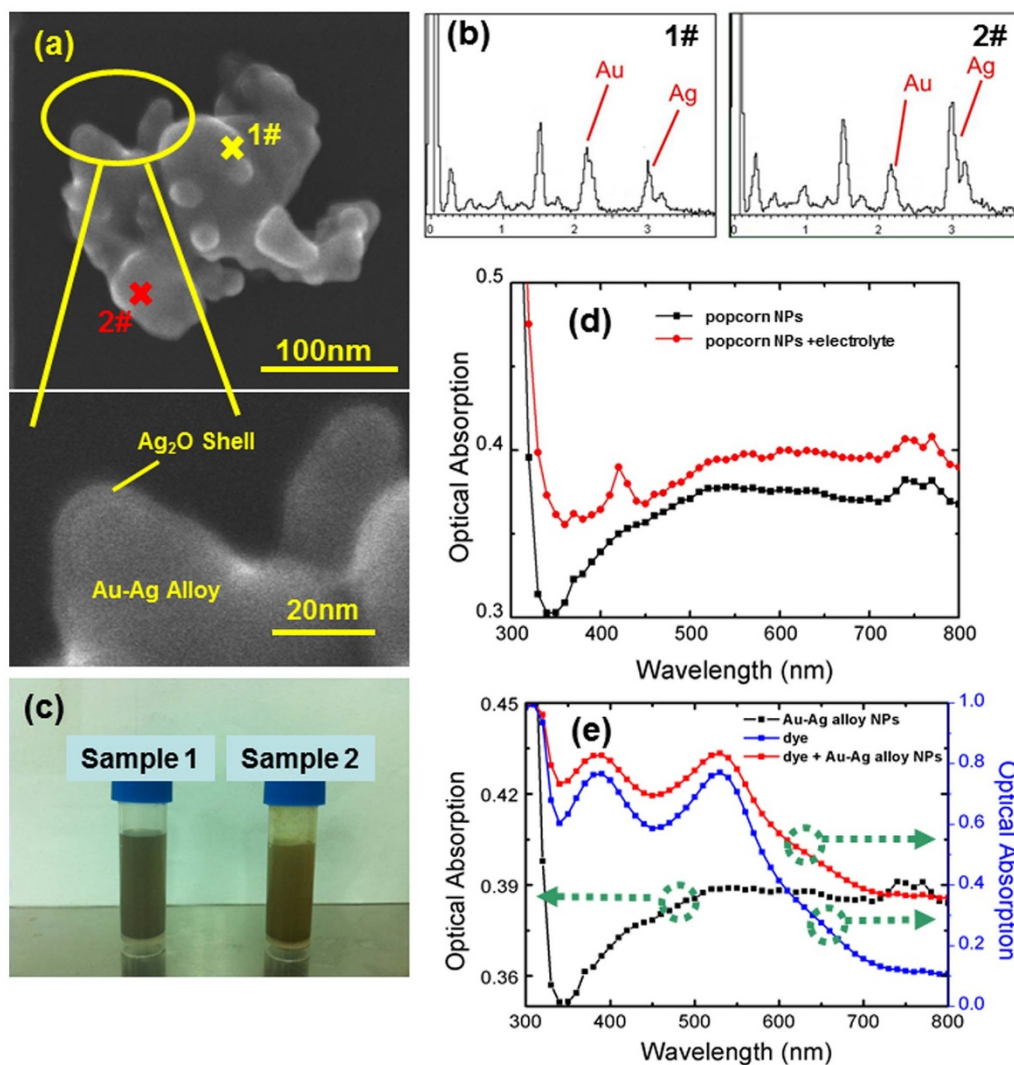


**Figure 3** | (a) Scanning electron microscopy (SEM) image of popcorn NPs. (b) Energy dispersive spectroscopy (EDS) of popcorn NPs refers to point 1# and point 2# in Fig. 3 (a). (c) Appearance of popcorn NPs with (sample 2)/without (sample 1) electrolyte. (d) Optical absorption of popcorn NPs before/after being mixed with electrolyte. (e) Optical absorption spectra of popcorn NPs (black curve), N719 dye molecules (blue curve), and a mixture of popcorn NPs and dye in ethanol solution (red curve).

of Au-Ag alloy popcorn NPs on the light absorption enhancement of dye molecules, we studied the light absorption of a dye with and without Au-Ag alloy popcorn NPs in ethanol solution. The light absorption of the dye molecules in the ethanol solution mixed with popcorn NPs was greatly enhanced due to LSP-based light trapping, as shown in Fig. 3(e).

Furthermore, the LSP effect of popcorn NPs on the light absorption enhancement of dye molecules in  $\text{TiO}_2$  films was investigated. Plasmonic anodes were fabricated by incorporating popcorn NPs into  $\text{TiO}_2$  films (see Methods). Figure 4(a) shows the SEM image of a plasmonic  $\text{TiO}_2$  film incorporated with popcorn NPs, from which we can observe that the popcorn NPs were located and well distributed in the  $\text{TiO}_2$  layer (See Fig. S3, Supporting information). The EDS results in Fig. 4(b) indicate the components and demonstrate the existence of the plasmonic NPs in the  $\text{TiO}_2$  film. The optical absorption spectra of dye-sensitized  $\text{TiO}_2$  films with and without popcorn NPs indicate the broadband optical absorption enhancement of dye molecules in the plasmonic anode, as shown in Fig. 4(c). The relative change ( $\Delta\text{OA}/\text{OA}$ ) in the light absorption spectrum of the dye is shown in Fig. 4(d). The curves present a broadband light absorption enhancement and increase sharply beginning at 550 nm. This result is consistent with the broadband

optical absorption of popcorn NPs shown in Fig. 3(d). Moreover, the popcorn NPs in  $\text{TiO}_2$  anode after  $500^\circ\text{C}$  annealed still perform a broadband LSP enhancement, which could also demonstrate the thermal stabilities of the popcorn NPs (See Fig. S4 Supporting information). It should be noted that around the two light absorption peaks of dye N719 at approximately 385 nm and 520 nm, the relative ( $\Delta\text{OA}/\text{OA}$ ) light absorption enhancement exhibits two troughs. These troughs can be explained by a theory stating that the light absorption enhancement of active materials exhibiting an LSP effect is less significant when the material's original absorption ability is high<sup>30</sup>.

To further investigate the performance of plasmonically enhanced popcorn NPs,  $\text{TiO}_2$ -only and plasmonic DSCs were fabricated and characterised. Table 1 shows the performance of DSCs of different compositions. The table clearly demonstrates that there is an enhancement in both the short-circuit current density ( $J_{sc}$ ) and PCE of the DSCs incorporated with certain concentrations of plasmonic popcorn NPs (1.09 wt% for device 2 and 2.38 wt% for device 3). However, when further increasing the concentration of plasmonic popcorn NPs (4.83 wt% for device 4), the fill factor ( $FF$ ) and  $J_{sc}$  of the devices decrease, which leads to a decline in the PCE. This decrease in performance may be caused by increased recombination of



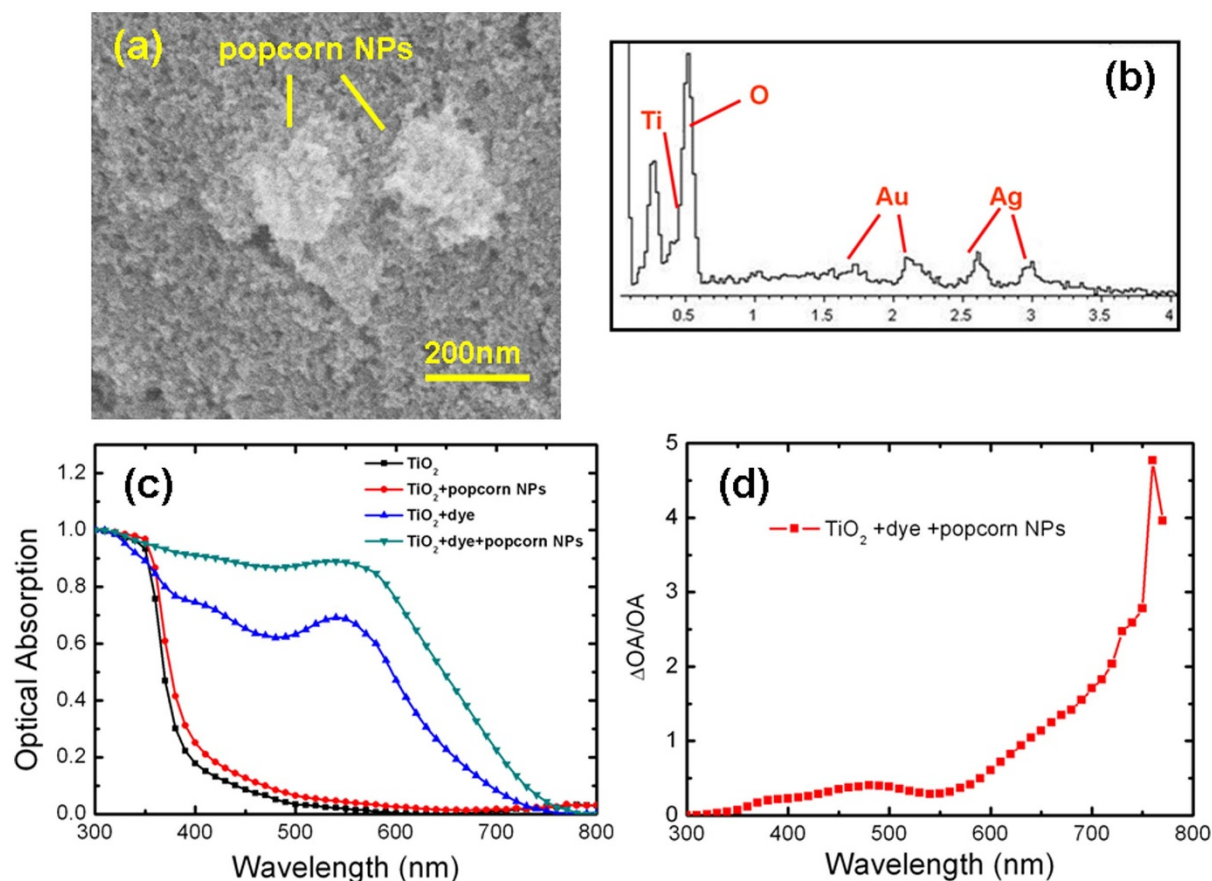


**Figure 4** | (a) Scanning electron microscopy (SEM) image of dye-sensitized TiO<sub>2</sub> film incorporated with popcorn NPs. (b) Energy dispersive spectroscopy (EDS) of TiO<sub>2</sub> film incorporated with popcorn NPs. (c) Optical absorption spectra of TiO<sub>2</sub> film with (red curve) or without popcorn NPs (black curve) and dye (N719) sensitized TiO<sub>2</sub> film with (green curve) or without popcorn NPs (blue curve). (d) Relative light absorption change ( $\Delta OA/OA$ ) of dye-sensitized TiO<sub>2</sub> film with popcorn NPs. The thickness of the film is 3  $\mu\text{m}$ . Here,  $\Delta OA(\lambda)/OA(\lambda) = (OA_{\text{TiO}_2+\text{dye}+\text{popcorn}}(\lambda) - OA_{\text{TiO}_2+\text{dye}}(\lambda))/OA_{\text{TiO}_2+\text{dye}}(\lambda)$ , where  $OA_{\text{TiO}_2+\text{dye}+\text{popcorn}}(\lambda)$  and  $OA_{\text{TiO}_2+\text{dye}}(\lambda)$  are the optical absorptions at wavelength  $\lambda$  of dye-sensitized TiO<sub>2</sub> films with and without popcorn NPs, respectively.

photo-generated electrons when high concentration of Au-Ag popcorn NPs are introduced.

The PCE of the plasmonic DSC with 2.38 wt% Au-Ag alloy popcorn NPs (device 3) reaches 6.09%, which indicates an enhancement of 16% compared with the PCE of the reference DSC (device 1). The current density versus voltage characteristics ( $J-V$  curves) are shown in Fig. 5(a). The  $V_{oc}$  and  $FF$  remain nearly unchanged, while the  $J_{sc}$  shows an obvious increase due to the LSP-enhanced optical absorption of the dye.

## Discussion

To further improve device performance, a polymeric reflective film was applied on the exterior of the counter electrode<sup>31</sup>. Based on the original device structure shown in Fig. 1, a white diffuse reflective film was added to the exterior of the counter electrode, which can be considered an opaque scattering layer, while keeping other

experimental parameters unchanged. The white diffuse reflective film can scatter the non-absorbed incident light back to the TiO<sub>2</sub> layer and hence improve the light absorption of DSCs. With the scattering layer, the popcorn NPs would be illuminated from different directions simultaneously, surrounding which the LSP modes would be excited more efficiently. Hence, the popcorn NPs would exhibit a more pronounced LSP effect, which would improve the light absorption, and plasmonic DSCs would exhibit a more significant enhancement in  $J_{sc}$  and PCE. The  $J-V$  curves of reference and plasmonic DSCs with a scattering layer are shown in Fig. 5(b). The  $J_{sc}$  increases from 13.07 mA/cm<sup>2</sup> to 19.51 mA/cm<sup>2</sup> due to the popcorn NPs, and the PCE of the plasmonic DSCs with a scattering layer reaches up to 7.85%, which represents a significant enhancement of 32% compared to the PCE of the reference device (5.94%, device 5), as shown in Table 1. This result indicates that by adding a scattering layer, the popcorn NPs have a stronger ability to enhance the

**Table 1** | The performance of DSCs of different compositions

Device	DSC composition	$V_{oc}$ (V)	$J_{sc}$ (mA/cm <sup>2</sup> )	FF (%)	PCE(%)
1	TiO <sub>2</sub> -only	0.703 ± 0.11	12.21 ± 0.01	61.3 ± 0.1	5.26 ± 0.1
2	1.09 wt% popcorn NPs	0.708 ± 0.13	13.50 ± 0.01	60.2 ± 0.1	5.75 ± 0.1
3	2.38 wt% popcorn NPs	0.699 ± 0.21	14.62 ± 0.02	59.6 ± 0.1	6.09 ± 0.1
4	4.83 wt% popcorn NPs	0.702 ± 0.14	13.38 ± 0.01	56.6 ± 0.2	5.32 ± 0.1
5	TiO <sub>2</sub> -only DSC with scattering layer	0.728 ± 0.23	13.07 ± 0.01	62.4 ± 0.2	5.94 ± 0.1
6	Plasmonic DSC with scattering layer	0.709 ± 0.08	19.51 ± 0.02	56.7 ± 0.1	7.85 ± 0.2

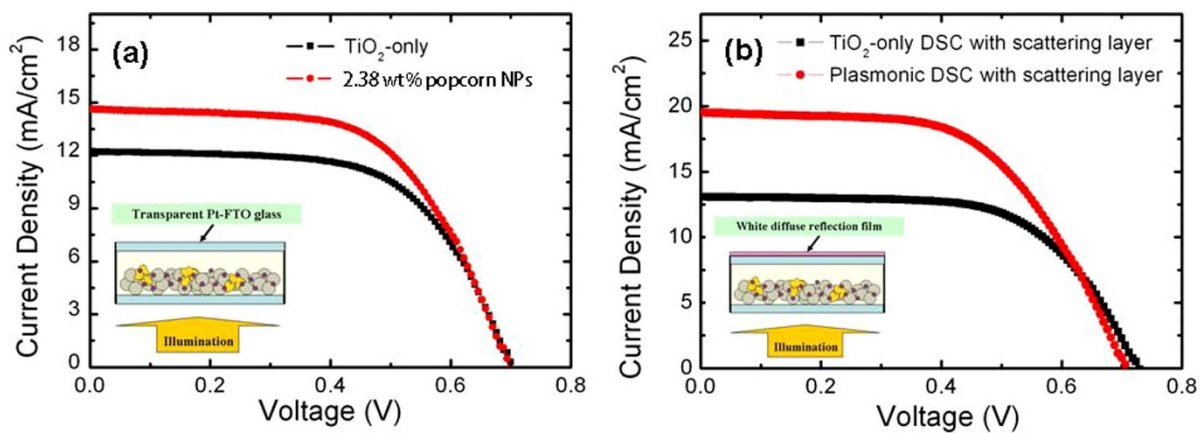


**Figure 5** | (a) The photocurrent density-voltage characteristics (J–V curves) of plasmonic DSCs incorporated with popcorn NPs at the optimised concentration of 2.38 wt% (device 3) and TiO<sub>2</sub>-only DSCs (device 1), (b) The J–V curves of plasmonic DSCs incorporated with popcorn NPs (device 6) and TiO<sub>2</sub>-only DSCs (device 5). Insets show the schematic structure of the DSCs with or without a reflection film.

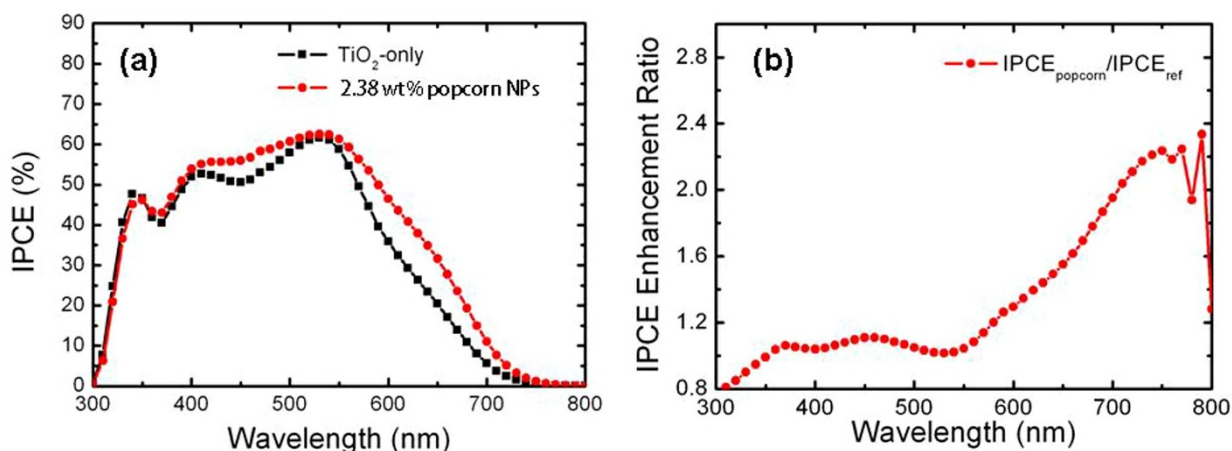
photocurrent and the efficiency of DSCs, which should result from the more efficient excitation of LSP modes on the popcorn NPs, thereby confirming the theoretical analysis shown in Fig. 2.

Figure 6(a) shows the IPCE spectra of TiO<sub>2</sub>-only DSCs (black curve) and Au–Ag alloy popcorn NP-enhanced DSCs (red curve). It is indicated that the IPCE of the popcorn NP-enhanced DSCs is enhanced over the entire wavelength range, which should be attributed to the light harvesting enhancement due to the LSP effect of popcorn NPs. The IPCE enhancement ratio of popcorn NP-enhanced DSCs to TiO<sub>2</sub>-only DSCs shown in Fig. 6(b) demonstrates that the enhancement is significant over the wavelength range of 520–800 nm. This phenomenon is consistent with the broadband LSP feature and the optical absorption enhancement of the popcorn NPs shown in Figs. 2(c) and 3(a). Therefore, the measured IPCE also confirms that the LSPs of Au–Ag alloy popcorn NPs improve DSC performance by providing a broad optical absorption enhancement of dye molecules.

In addition to the LSP effect of the popcorn NPs, a scattering effect will also exist, which should also contribute to the light absorption enhancement of DSCs<sup>32</sup>. However, we believe that the LSP effect dominates the enhancement of light absorption due to the following reasons. (1) The fine structures of the popcorn NPs measure approximately 20–40 nm; thus, the LSP modes would be excited more

efficiently on these fine structures as shown in Fig. 2 compared with those of regular NPs without fine structures. According to Mie theory<sup>33</sup>, when the LSP mode is efficiently excited, the scattering effect is relatively low. (2) The light absorption enhancement afforded by scattering effect is not considerable if only the NP concentration is high, which is several times that incorporated into LSP-enhanced DSCs<sup>24</sup>. In this study, we obtained a significant PCE enhancement of 32% with a low concentration of popcorn NPs; hence, we believe that the light absorption enhancement of DSCs is mainly due to the LSP effect of the plasmonic popcorn NPs.

Electrochemical analysis of the DSCs were performed to gain deeper insights into the interactions between both components. Figure 7(a) shows the cyclic voltammogram measurement of N719 sensitized TiO<sub>2</sub> anode incorporated without and with 2.38 wt% popcorn NPs. From the figure we can observe that the oxidation and reduction potential of dye N719 in the presence of the popcorn NPs remain almost unchanged, compared with that in the absence of the popcorn NPs. This indicates that the PCE enhancement of plasmonic DSCs has no direct relation with the redox behaviour of the dye molecules. The boost in  $J_{sc}$  of plasmonic DSC leads to the PCE enhancement, which is result from the light absorption improvement of dye molecules by popcorn NPs. Electrochemical impedance spectra (EIS) provide the insight into the operation mechanism, as shown



**Figure 6** | (a) Incident photon-to-electron conversion efficiency (IPCE) of DSCs incorporated with popcorn NPs at optimised concentration of 2.38 wt% (device 3) and TiO<sub>2</sub>-only DSCs (device 1). (b) The IPCE enhancement ratio of the plasmonic DSCs (device 3). IPCE enhancement ratio =  $(IPCE_{\text{popcorn}}(\lambda)/IPCE_{\text{TiO}_2\text{-only}}(\lambda))$ , where  $IPCE_{\text{popcorn}}(\lambda)$  and  $IPCE_{\text{TiO}_2\text{-only}}(\lambda)$  are the IPCEs of the popcorn NP-enhanced DSCs and TiO<sub>2</sub>-only DSCs at wavelength  $\lambda$ , respectively.

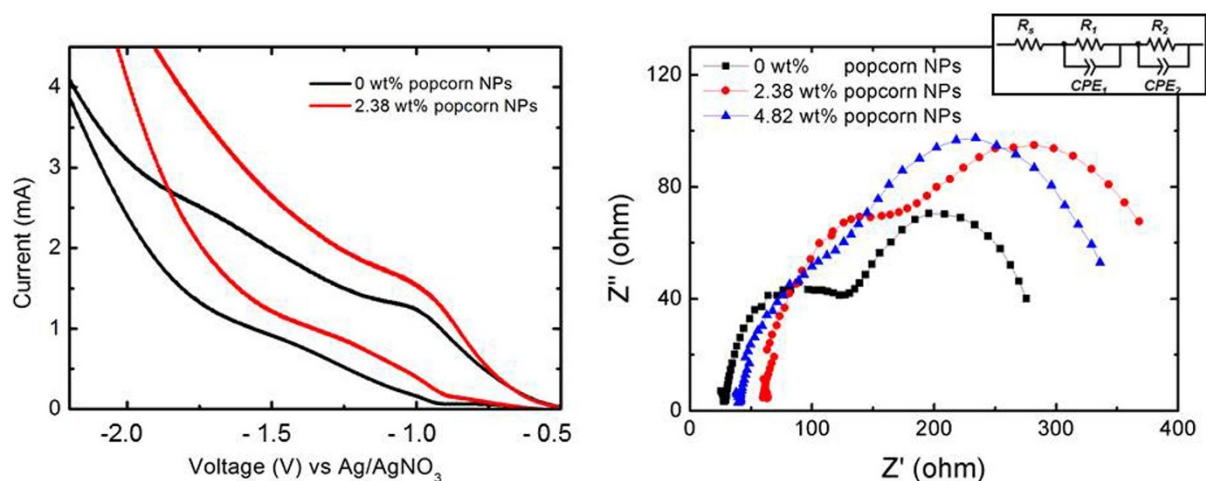


**Figure 7** | (a) Cyclic voltammogram of N719 sensitized TiO<sub>2</sub> anode incorporated with/without popcorn NPs measured at a sweep rate of 200 mV/s. (b) Electrochemical impedance spectra of DSCs incorporated with popcorn NPs of different concentrations. Inset is The equivalent circuit.

in Fig. 7(b), where  $R_s$ ,  $R_1$  and  $R_2$  represent the series resistance, charge transfer resistance on counter electrode and at the interface of TiO<sub>2</sub>/dye/electrolytes<sup>24</sup>. In EIS spectrum, the  $R_s$  of DSCs with 0 wt% (device 1 in Table 1), 2.38 wt% (device 2) and 4.83 wt% (device 3) is 27.1  $\Omega$ , 38.6  $\Omega$  and 60.1  $\Omega$ , respectively. The increased  $R_s$  is a result of popcorn NPs incorporation, since the only difference is the different concentrations. Moreover, the diameters of the Nyquist semi-circles correspond to charge transfer resistance ( $R_2$ ) at the TiO<sub>2</sub>/dye/electrolyte interfaces. Owing to the work function of Ag<sub>2</sub>O shell is higher than that of TiO<sub>2</sub> and the metal core act as combination centres, popcorn NPs with Ag<sub>2</sub>O shell existed in TiO<sub>2</sub> anode would lead to an increase in the charge transfer resistance for higher  $R_2$  as well as  $R_s$ . These resistances are negative effects in the DSCs performance improvement, therefore, the popcorn NPs of an optimized concentration is essential for the plasmonic DSCs.

In summary, Au-Ag alloy popcorn core-shell NP-enhanced DSCs were proposed and realised. It was demonstrated numerically that due to the fine structures on popcorn NPs of different size and shape and with different proportions of Au and Ag, LSP modes at different wavelengths could be excited simultaneously around the popcorn NPs, as revealed by the measured broadband light absorption of popcorn NP solutions. By introducing popcorn NPs at the optimised concentration of 2.38 wt%, the PCE of DSCs was enhanced by 16%, from 5.26% to 6.09%. Moreover, by adding a scattering layer on the exterior of the counter electrode of the DSCs, the popcorn NPs demonstrate a stronger ability to enhance the photocurrent and efficiency of DSCs. The PCE of DSCs was improved by 32%, from 5.94% to 7.85%, which results from the more efficient excitation of LSP modes on the popcorn NPs.

## Methods

**Numerical calculations.** Instead of 3D models, 2D models based on the finite element method (FEM) were established for simplicity. In this study, the COMSOL software program (RF Module, COMSOL Multiphysics 3.5a) adopting the FEM to solve the Maxwell equations was applied to calculate the LSP modes supported by a popcorn NP at different wavelengths. The popcorn NP was located in a rectangular area (800 nm  $\times$  2  $\mu$ m) with side and bottom boundaries both set as absorbing boundaries. The popcorn NP was assumed to be an ellipsoidal structure (prolate and minor axes measuring 180 nm and 80 nm, respectively) with several small ellipsoidal structures (ranging in size from 20 to 50 nm) on it. The NP material was set to be solely gold for simplicity and the surrounding material was set to be TiO<sub>2</sub>. The optical properties of gold and TiO<sub>2</sub>, including the wavelength-dependent refractive index  $n$  and extinction coefficient  $k$ , were obtained from the literature<sup>34</sup>. Incident light with wavelength  $\lambda_0$  was set to simulate solar light. Varying  $\lambda_0$ , LSP modes at different wavelengths were demonstrated.

**Synthesis of NPs.** To fabricate the popcorn NPs, a modified two-step co-reduction synthesis procedure was implemented, which was developed based on the

conventional co-reduction method<sup>29</sup>. First, a 100 mL aqueous solution containing 0.038 g HAuCl<sub>4</sub> and 0.068 g AgNO<sub>3</sub> (both purchased from Sigma-Aldrich) was heated to 97°C (close to its boiling point) under vigorous stirring at 400 rpm in an oil bath system; then, 2 ml of a 1 wt% sodium citrate (purchased from Sigma-Aldrich) solution was injected quickly into the solution to react for 8 minutes. The solution turned dark red and then dark yellow. The temperature of the heating system was then adjusted to 150°C to make the solution boil rapidly, and 2 ml of a 5 wt% sodium citrate solution was added; the reaction was allowed to continue for another 30 minutes. The solution turned dark grey. Finally, the solution was cooled down to room temperature with stirring, and the NPs were collected by centrifugation at 3,300 rpm and redispersed in ethanol by sonicating for 5 minutes.

**Characterisation of NPs.** Scanning electron microscopy (SEM, HITACHI S-5500, 30 kV) images and energy dispersive spectroscopy (EDS, Horiba EX-250) spectra of the popcorn NPs and TiO<sub>2</sub> layer were obtained. The optical absorption spectroscopy measurements were performed using a HITACHI U-3010 UV-visible spectrophotometer. To gain further insights into the film composition, 3  $\mu$ m TiO<sub>2</sub> films incorporated with and without popcorn NPs were fabricated on FTO glass or silica wafers by spin coating (SC-1B, Jinshengweina Co., Ltd.), followed by annealing at 500°C for 20 min. These films were used for optical absorption measurements and SEM characterisation. The film thickness was measured using a Dektak 150 surface profiler. The films were immersed in a 0.1 mM dye (N719, purchased from Dyesol) ethanol solution for 24 h at room temperature and were then washed with ethanol to remove the non-adsorbed dye molecules, followed by natural air drying.

**Fabrication of DSCs.** To fabricate photoanodes of plasmonic DSCs, 0.12 g TiO<sub>2</sub> paste (purchased from Dyesol) was dispersed in 1.5 mL ethanol, mixed with a popcorn NP ethanol solution and stirred sufficiently. The ratio of plasmonic NPs to TiO<sub>2</sub> could be readily adjusted by changing the concentration of Au-Ag alloy popcorn NPs in solution. The plasmonic TiO<sub>2</sub> paste was spin-coated on a FTO glass substrate at 1800 rpm for 30 seconds and dried at 125°C for 5 min. This procedure was repeated 3 times to increase the thickness of the TiO<sub>2</sub> layer. Then, the TiO<sub>2</sub> photoanode was annealed at 500°C for 15 min. A TiO<sub>2</sub>-only photoanode was also prepared by mixing the TiO<sub>2</sub> paste with ethanol in the same proportion for comparison. The thickness of both the TiO<sub>2</sub>-only and plasmonic TiO<sub>2</sub> layer were measured using a Dektak 150 surface profiler and fixed at  $\sim$ 8  $\mu$ m by controlling the preparation conditions. These photoanodes were immersed in a 0.1 mM dye (N719, purchased from Dyesol) ethanol solution and kept at room temperature for 24 h. Then, the impregnated photoanodes were placed in ethanol for 5 min to remove the non-adsorbed dye, followed by natural drying in air. Finally, the device was sealed by a sealing frame (Surlyn sealant) and injected with electrolyte (EL-HPE, Dyesol). The electrolyte mainly consisted of I<sub>2</sub> and LiI in an acetonitrile solvent.

For the SEM and optical absorption measurements of the TiO<sub>2</sub> films, a similar fabrication method was employed. The thickness of the TiO<sub>2</sub> films could be readily adjusted by controlling the number of times spin coating was repeated.

**Electrochemical characterisation of DSCs.** Cyclic voltammetry of dye N719 bound to TiO<sub>2</sub> anode with or without popcorn NPs was performed in 0.1 M tetrabutylammonium hexafluorophosphate (Aldrich, TBAH) dichloromethane electrolyte. An electrochemical workstation (CHI 660D) was used in a standard three-cell arrangement consisting of a modified TiO<sub>2</sub> electrode as working electrode, a Pt gauze as counterelectrode, and a Ag/AgNO<sub>3</sub> as reference electrode. The scan rate was set to be 200 mV/s.

Electrochemical impedance spectroscopy (EIS) was recorded over a frequency range of 1 to 10000 Hz with an AC amplitude of 5 mV by using electrochemical





workstation (CHI 604A). The initial potential was set to be  $-0.65$  V and the quiet time was 2 sec. The parameters were calculated from Z-View software (v2.1b, Scribner Associates, Inc.)

**Photovoltaic characterisation of DSCs.** The current-voltage characteristics of DSCs were measured under AM 1.5 G illumination using a solar simulator (XEC-300M2, SAN-EL, Japan). The power of the simulated light was calibrated to  $1,000$  W/m<sup>2</sup> using a standard reference Si solar cell, and I-V curves were obtained by applying an external bias to the cell and measuring the generated photocurrent with a digital source meter (KEITHLEY 2400, USA). The voltage step and delay time of the photocurrent were 6 mV and 30 ms, respectively. To investigate the light absorption enhancement based on the LSP effect at different wavelengths, the spectral response of the solar cells was observed by using an IPCE measurement system (QEX10, PV Measurement, USA) consisting of a 150 W xenon lamp light source. The incident photon flux was also determined by using a calibrated silicon photodiode.

- O'Regan, B. & Grätzel, M. A. Low-Cost, High-Efficiency Solar Cell Based on Dye-Sensitized Colloidal TiO<sub>2</sub> Films. *Nature* **353**, 737–740 (1991).
- Nazeeruddin, M. K. *et al.* Conversion of Light to Electricity by cis-X2bis (2,20-bipyridyl-4,40-dicarboxylate) ruthenium(II) Charge-Transfer Sensitizers (X = Cl-, Br-, I-, CN-, and SCN-) on Nanocrystalline Titanium Dioxide Electrodes. *J. Am. Chem. Soc.* **115**, 6382–6390 (1993).
- Grätzel, M. Photoelectrochemical cells. *Nature* **414**, 338–344 (2001).
- Grätzel, M. Dye-sensitized solar cells. *J. Photochem. Photobiol. Photochem. Rev.* **4**, 145–153 (2003).
- Hamann, T. W., Jensen, R. A., Martinson, A. B. F., Ryswyk, H. V. & Hupp, J. T. Advancing beyond current generation dye-sensitized solar cells. *Energy & Environmental Science* **1**, 66–78 (2008).
- Alvarez-Puebla, R., Liz-Marzan, L. M. & Garcia de Abajo, F. J. Light Concentration at the Nanometer Scale. *J. Phys. Chem. Lett.* **1**, 2428–2434 (2010).
- Nabika, H., Takase, M., Nagasawa, F. & Murakoshi, K. Toward Plasmon-Induced Photoexcitation of Molecules. *J. Phys. Chem. Lett.* **1**, 2470–2487 (2010).
- Koh, A. L., Fernández-Domínguez, A. I., McComb, D. W., Maier, S. A. & Yang, J. K. W. High-Resolution Mapping of Electron-Beam-Excited Plasmon Modes in Lithographically Defined Gold Nanostructures. *Nano Lett.* **11**, 1323–1330 (2011).
- Slaughter, L., Chang, W. S. & Link, S. Characterizing Plasmons in Nanoparticles and Their Assemblies with Single Particle Spectroscopy. *J. Phys. Chem. Lett.* **2**, 2015–2023 (2011).
- Blaber, M. G., Henry, A. I., Bingham, J. M., Schatz, G. C. & Van Duyne, R. P. LSPR Imaging of Silver Triangular Nanoprisms: Correlating Scattering with Structure Using Electrodynamics for Plasmon Lifetime Analysis. *J. Phys. Chem. C* **116**, 393–403 (2012).
- Thimsen, E., Le Formal, F., Grätzel, M. & Warren, S. C. Influence of plasmonic Au nanoparticles on the photoactivity of Fe<sub>2</sub>O<sub>3</sub> electrodes for water splitting. *Nano Lett.* **11**, 35–43 (2011).
- Noguez, C. Surface Plasmons on Metal Nanoparticles: The Influence of Shape and Physical Environment. *J. Phys. Chem. C* **111**, 3806–3819 (2007).
- Ihara, M., Tanaka, K., Sakaki, K., Honma, I. & Yamada, K. Enhancement of the Absorption Coefficient of cis-(NCS)<sub>2</sub> Bis(2,20-bipyridyl-4,40-dicarboxylate) ruthenium(II) Dye in Dye-Sensitized Solar Cells by a Silver Island Film. *J. Phys. Chem. B* **101**, 5153–5157 (1997).
- Ishikawa, K., Wen, C. J., Yamada, K. & Okubo, T. The Photocurrent of Dye-Sensitized Solar Cells Enhanced by the Surface Plasmon Resonance. *J. Chem. Eng. of Jpn.* **37**, 645–649 (2004).
- Hagglund, C., Zach, M. & Kasemo, B. Enhanced Charge Carrier Generation in Dye Sensitized Solar Cells by Nanoparticle Plasmons. *Appl. Phys. Lett.* **92**, 013113 (2008).
- Standridge, S. D., Schatz, G. C. & Hupp, J. T. Toward Plasmonic Solar Cells: Protection of Silver Nanoparticles Via Atomic Layer Deposition of TiO<sub>2</sub>. *Langmuir* **25**, 2596–2600 (2009).
- Standridge, S. D., Schatz, G. C. & Hupp, J. T. Distance Dependence of Plasmon-Enhanced Photocurrent in Dye-Sensitized Solar Cells. *J. Am. Chem. Soc.* **131**, 8407–8409 (2009).
- Zhao, G., Kozuka, H. & Yoko, T. Effects of the Incorporation of Silver and Gold Nanoparticles on the Photoanodic Properties of Rose Bengal Sensitized TiO<sub>2</sub> Film Electrodes Prepared by Sol-Gel Method. *Sol. Energy Mater. Sol. Cells* **46**, 219–231 (1997).
- Wen, C., Ishikawa, K., Kishima, M. & Yamada, K. Effects of Silver Particles on the Photovoltaic Properties of Dye-Sensitized TiO<sub>2</sub> Thin Films. *Sol. Energy Mater. Sol. Cells* **61**, 339–351 (2000).
- Brown, M. D. *et al.* Plasmonic Dye-Sensitized Solar Cells Using Core-Shell Metal-Insulator Nanoparticles. *Nano Lett.* **11**, 438–445 (2011).
- Qi, J., Dang, X., Hammond, P. T. & Belcher, A. M. Highly Efficient Plasmon-Enhanced Dye-Sensitized Solar Cells Through Metal@Oxide Core@Shell Nanostructure. *ACS Nano* **5**, 7108–7116 (2011).
- Xu, Q., Liu, F., Meng, W. & Huang, Y. Plasmonic core-shell metal-organic nanoparticles enhanced dye-sensitized solar cells. *Opt. Express* **20**, A898–A907 (2012).
- Dang, X. *et al.* Tunable localized surface plasmon-enabled broadband light harvesting enhancement for high-efficiency panchromatic dye-sensitized solar cells. *Nano Lett.* **13**, 637–642 (2013).
- Chang, S., Li, Q., Xiao, X., Wong, Y. K. & Chen, T. Enhancement of Low Energy Sunlight Harvesting in Dye-Sensitized Solar Cells Using Plasmonic Gold Nanorods. *Energy Environ. Sci.* (2012).
- Zayats, A. V., Smolyaninov, I. I. & Maradudin, A. A. Nano-optics of surface plasmon polaritons. *Physics reports* **408**, 131–314 (2005).
- Shen, H., Bienstman, P. & Maes, B. Plasmonic absorption enhancement in organic solar cells with thin active layers. *J. Appl. Phys.* **106**, 073109 (2009).
- Moulé, A. J. *et al.* Optical description of solid-state dye-sensitized solar cells. I. Measurement of layer optical properties. *J. Appl. Phys.* **106**, 073111 (2009).
- Ito, S. *et al.* Fabrication of thin film dye sensitized solar cells with solar to electric power conversion efficiency over 10%. *Thin Solid Films* **516**, 613–4619 (2008).
- Wang, D. & Li, Y. Bimetallic Nanocrystals: Liquid-Phase Synthesis and Catalytic Applications. *Adv. Mater.* **23**, 1044–1060 (2011).
- Khurgin, J. B., Sun, G. & Soref, R. A. Practical limits of absorption enhancement near metal nanoparticles. *Appl. Phys. Lett.* **94**, 071103 (2009).
- Lee, J. Y. *et al.* Simple approach for enhancement of light harvesting efficiency of dye-sensitized solar cells by polymeric mirror. *Opt. Express* **18**, A522–A527 (2010).
- Chen, X. *et al.* Broadband enhancement in thin-film amorphous silicon solar cells enabled by nucleated silver nanoparticles. *Nano Lett.* **12**, 2187–2192 (2012).
- Jain, P. K., Huang, X., El-Sayed, I. H. & El-Sayed, M. A. Review of Some Interesting Surface Plasmon Resonance enhanced Properties of Noble Metal Nanoparticles and Their Applications to Biosystems. *Plasmonics* **2**, 107–118 (2007)
- Ferber, J. & Luther, J. Computer simulations of light scattering and absorption in dye-sensitized solar cells. *Sol. Energy Mater. Sol. Cells* **54**, 265–275 (1998).

## Acknowledgments

This work was supported by the National Basic Research Programs of China (973 Program) under Contracts No. 2013CBA01704, 2010CB327405 and 2011CBA00608; the National High-tech R&D Program (863 Program) under Contract No. 2011AA050504; and the National Natural Science Foundation of China (NSFC-61036011, NSFC-61107050, and NSFC-61036010). The Authors also want to thank Hong Lin from Department of Material Science and Engineering, Tsinghua University, for her kindly and important guidelines on this work.

## Author contributions

Y.H. and F.L. conceived the project. F.L. and Q.X. planned the experiments. Q.X. and Y.L. carried out the simulation and experiment. Q.X., F.L. and Y.H. co-wrote the manuscript. W.Z., K.C., X.F. and Y.H. were involved in interpretation of the result and commented on the manuscript at all stages

## Additional information

**Supplementary information** accompanies this paper at <http://www.nature.com/scientificreports>

**Competing financial interests:** The authors declare no competing financial interests.

**How to cite this article:** XU, Q. *et al.* Broadband light absorption enhancement in dye-sensitized solar cells with Au-Ag alloy popcorn nanoparticles. *Sci. Rep.* **3**, 2112; DOI:10.1038/srep02112 (2013).



This work is licensed under a Creative Commons Attribution-NonCommercial-NoDerivs 3.0 Unported license. To view a copy of this license, visit <http://creativecommons.org/licenses/by-nc-nd/3.0>